Global satellite-observed daily vertical migrations of ocean animals

Behrenfeld Michael J. [1, *], Gaube Peter [2], Della Penna Alice [2, 3], O'malley Robert T. [1], Burt William J. [4, 5], Hu Yongxiang [6], Bontempi Paula S. [7], Steinberg Deborah K. [8], Boss Emmanuel S. [9], Siegel David A. [10, 11], Hostetler Chris A. [6, 12], Tortell Philippe D. [4], Doney Scott C. [13]

[1] Department of Botany and Plant Pathology, Oregon State University, Corvallis, OR, USA
[2] Applied Physics Laboratory, Air-Sea Interaction and Remote Sensing Department, University of Washington, Seattle, WA, USA
[3] Laboratoire des Sciences de l'Environnement Marin (LEMAR), UMR 6539 CNRS-Ifremer-IRD-UBO-Institut Universitaire Européen de la Mer (IUEM), Plouzané, France
[4] Earth, Ocean and Atmospheric Sciences, University of British Columbia, Vancouver, British Columbia, Canada
[5] College of Fisheries and Ocean Sciences, University of Alaska Fairbanks, Fairbanks, AK, USA
[6] NASA Langley Research Center, Hampton, VA, USA
[7] Earth Science Division, Science Mission Directorate, National Aeronautics and Space Administration Headquarters, Washington, DC, USA
[8] Virginia Institute of Marine Science, College of William & Mary, Gloucester Point, VA, USA
[9] School of Marine Sciences, University of Maine, Orono, ME, USA
[10] Earth Research Institute, University of California Santa Barbara, Santa Barbara, CA, USA
[11] Department of Geography, University of California Santa Barbara, Santa Barbara, CA, USA
[12] Botany Department, University of British Columbia, Vancouver, British Columbia, Canada
[13] Department of Environmental Sciences, University of Virginia, Charlottesville, VA, USA

* Corresponding author : Michael J. Behrenfeld, email address : mjb@science.oregonstate.edu

Abstract :

Every night across the world's oceans, numerous marine animals arrive at the surface of the ocean to feed on plankton after an upward migration of hundreds of metres. Just before sunrise, this migration is reversed and the animals return to their daytime residence in the dark mesopelagic zone (at a depth of 200–1,000 m). This daily excursion, referred to as diel vertical migration (DVM), is thought of primarily as an adaptation to avoid visual predators in the sunlit surface layer[1,2] and was first recorded using ship-net hauls nearly 200 years ago[3]. Nowadays, DVMs are routinely recorded by ship-mounted acoustic systems (for example, acoustic Doppler current profilers). These data show that night-time arrival and departure times are highly conserved across ocean regions[4] and that daytime descent depths increase with water clarity[4,5], indicating that animals have faster swimming speeds in clearer waters[4]. However, after decades of acoustic measurements, vast ocean areas remain unsampled and places for which data are available typically provide information for only a few months, resulting in an incomplete understanding of DVMs. Addressing this issue is important, because DVMs have a crucial role in global ocean biogeochemistry. Night-time feeding at the surface and daytime metabolism of this food at depth provide

an efficient pathway for carbon and nutrient export6,7,8. Here we use observations from a satellite-mounted light-detection-and-ranging (lidar) instrument to describe global distributions of an optical signal from DVM animals that arrive in the surface ocean at night. Our findings reveal that these animals generally constitute a greater fraction of total plankton abundance in the clear subtropical gyres, consistent with the idea that the avoidance of visual predators is an important life strategy in these regions. Total DVM biomass, on the other hand, is higher in more productive regions in which the availability of food is increased. Furthermore, the 10-year satellite record reveals significant temporal trends in DVM biomass and correlated variations in DVM biomass and surface productivity. These results provide a detailed view of DVM activities globally and a path for refining the quantification of their biogeochemical importance.

67   For decades, airplane-mounted light-detection-and-ranging (lidar) instruments have used the

68   backscattering of light (*bbp*) from phytoplankton, zooplankton, and small fish to locally map the

69   distribution of these organisms in the water column[9-11]. Unlike passive ocean sensors that

70   measure reflected sunlight, lidar uses lasers as a light source and thus has the capacity to measure

71   marine organisms both day and night. When DVM animals are prominent, their nocturnal

72   invasion of the surface ocean is expected to increase *bbp* at night compared to what it would be

73   in their absence. Five ship-based examples[12] of this DVM signature are shown in figure 1a,

74   where the animal signals contribute 7% to 28% of total nighttime *bbp*. These signals appear as

75   large spikes in this record because DVM animals are 'bright' targets compared to the

76   phytoplankton and other suspended particles constituting the much lower *bbp* baseline[13] [purple

77   line in Fig. 1a], but the animals are also rarer and only occasionally pass through the small

78   sample volume (~2 ml) of the ship's *bbp* instrument. In contrast, a lidar with a much larger

79   sampling volume can effectively capture the signal of all scattering components with every

80   measurement. The satellite Cloud-Aerosol Lidar with Orthogonal Polarization (CALIOP) sensor

81   has been conducting such measurements for over a decade[14-15] [Methods] and its *bbp* retrievals

82   provide an opportunity to decipher global patterns in vertically migrating animals.

83

84   The laser footprint of CALIOP has a diameter of 100 m at the ocean surface and a vertical

85   sampling depth of 22 m in water. What this means is that each CALIOP measurement integrates

86   the *bbp* signal from a water volume of 1.73×10^5 m^3, which is $\sim 5 \times 10^6$ greater than the entire water

87   volume measured over a given night in the field data shown in figure 1a. CALIOP's large

88   sampling volume thus ensures that each retrieved *bbp* value encompasses both the animals and

89   suspended cells and particles in the surface layer. CALIOP is a polar orbiting sensor that

90   conducts daytime and nighttime (~1:40 p.m. and a.m. local time, respectively) near-nadir

91   backscattering measurements along its orbit track at a sampling frequency equivalent to every

92   330 m on the ground.   A slightly precessing orbit with a 16-day repeat cycle provides global *bbp*

93   coverage, but ground tracks oriented in opposite directions on the daylight and dark sides of the

94   Earth mean that day and night *bbp* samples are rarely spatially coincident within a given 24 h

95   period [Extended Data Fig. 1, Supplementary Discussion]. The global signature of DVM

96   animals was therefore investigated by creating 2º latitude by 2º longitude binned monthly

97   CALIOP daytime (bbp^{day}) and nighttime (bbp^{night}) values of *bbp*.

98

99   In the absence of any DVM, the biomass-normalized *bbp* difference ratio:

100                    $$\Delta bbp = (bbp^{night} - bbp^{day}) / bbp^{day} \qquad\qquad (1)$$

101   is expected to yield a negative value for the measurement times of CALIOP [vertical red dotted

102   lines in Fig. 1b]. This is because daytime increases in phytoplankton cell size and organic

103   carbon content and nighttime cell division and metabolism[16-18] create a baseline diel cycle in

104   biomass-normalized *bbp* with an afternoon maximum and nighttime minimum [Fig. 1b][19]. The

105   presence of DVM animals increases bbp^{night} [Fig. 1a] and therefore causes Δbbp to become less

106   negative than the phytoplankton-only signal, or even positive if the migrators are sufficiently

107   abundant. Thus, phytoplankton and DVM animals together determine Δbbp [Fig. 1c], where the

108   magnitude and sign of Δbbp is an index of the DVM signal strength relative to that of the

109   phytoplankton.

110

111   The 2008 to 2017 CALIOP record reveals broad, spatially-coherent patterns in climatological

112   average Δbbp at tropical and subtropical latitudes [equatorward of the yellow/black lines in Fig.

113   2] where plankton populations are relatively stable in time due to the water column being

114   permanently stratified within the euphotic zone (referred to hereafter as the permanently

115   stratified ocean; PSO). These eight broad features [black outlines in Fig. 2] correspond to the

116   seasonally-varying boundaries of the North Pacific (NPSG), South Pacific (SPSG), North

117   Atlantic (NASG), South Atlantic (SASG), and South Indian (SISG) Subtropical Gyres and the

118   higher-nutrient Tropical Pacific (TP) and North Tropical (NTA) and South Tropical (STA)

119   Atlantic [Fig. 2, 3a, Extended Data Fig. 2]. Within these regions, Δbbp values are persistently

120   positive in the NPSG, persistently negative in the TP and NTA, and strongly seasonal in the

121   NASG, STA, and all three Pacific areas [Extended Data Fig. 3]. In the high-latitude seasonal

122   seas [poleward of the yellow/black line in Fig. 2], the CALIOP record reveals large

123   climatological average values for Δbbp. However, persistent cloud cover and small-scale spatio-

124   temporal variations in plankton populations in these regions cause within-bin mismatches in

125   bbp^{day} and bbp^{night} data to yield significant bin-to-bin variability in Δbbp [Supplementary

126   Discussion]. From this point forward, therefore, our analysis primarily focuses on the eight

127   regions of the PSO.

128

129   If variability in Δbbp is largely a reflection of DVM strength rather than changes in the

130   phytoplankton cycle, then results shown in figure 2 suggest significant regional differences in the

131   relative nighttime abundance of these animals. To test this DVM-basis of the regional patterns,

132   we compared CALIOP data to historical field ADCP observations of paired day (I_{dB}^{day}) and night

133   (I_{dB}^{night}) acoustic backscatter. Due to the sparsity of such data, it was necessary to aggregate 32

134   years (1985 to 2017) of field measurements into monthly 5° latitude by 5° longitude bins to

135   achieve even reasonable global coverage. [Methods]. We then calculated median values of the

136   normalized difference ratio:

137   $$\Delta B_{ADCP} = (I_{dB}^{night} - I_{dB}^{day}) / I_{dB}^{day}. \qquad (2)$$

138   CALIOP bbp data were then reaggregated into equivalent 5° x 5° bins and regional median

139   values of Δbbp were calculated using only those calendar months and bins for which ADCP data

140   were available. Comparison of ΔB_{ADCP} and Δbbp for all bins within our eight PSO regions

141   yielded a statistically significant relationship (p = 0.001, n = 331) [Fig. 3b, red line] with a slope

142   very similar to that calculated from regionally-averaged values for the six regions where ADCP

143   data identify a significant DVM signal [Fig. 3b, dashed line] [Supplementary Discussion]. In

144   other words, the ADCP and lidar data sets both indicate DVM animals constitute a greater

145   fraction of nighttime plankton communities in the optically-clear subtropical gyres that are most

146   advantageous to visual predators. Interestingly, the regionally-averaged data for the SISG and

147   SASG deviate from the other PSO regions [Fig. 3b]. The reason for this difference is unknown.

148   These are the only two regions where ΔB_{ADCP} is near zero, suggesting either few DVM animals

149   or that the influx of nighttime DVM animals is compensated by reverse-DVM animals leaving

150   the surface layer[20]. CALIOP data, in contrast, suggest a moderate DVM signal in the SISG and

151   SASG [Fig. 3b]. Perhaps the discrepancy in these two regions is simply due to poor ADCP

152   coverage (typically one day-night observation per 5º x 5º bin for the 32 year field record).

153   However, it is also noteworthy that all of the ADCP data in the SASG and all but eight

154   observations in the SISG predate the CALIOP mission, so a temporal change in DVM

155   populations cannot be ruled out.

156

157   Day and night zooplankton net tows provide quantitative field measurements of DVM biomass,

158   but these labor-intensive measurements are rarely collected at regular intervals over long periods.

159   Two exceptions in the PSO are the sustained records at the Hawaii Ocean Time-series (HOT)

160   site (22º 45'N, 158ºW)[21] and the Bermuda Atlantic Time Series (BATS) site (31º 40'N, 64º

161   10'W)[22] [yellow stars in Fig. 3a]. Despite considerable interannual variability, significant ($p <$

162   0.01) seasonal cycles in DVM biomass (g dry weight m^{-2}) are observed at these locations. For

163   the CALIOP bin centered on the HOT site, the seasonal cycle in Δbbp from January through

164   November is significantly correlated ($r^2 = 0.44$, $p = 0.03$) with field observations [Fig. 3c].

165   Likewise, Δbbp for the CALIOP bin centered on the BATS site exhibits a two-peaked seasonal

166   cycle that is well correlated with field observations from August through June ($r^2 = 0.42$, $p =$

167   0.03) [Fig. 3d]. These results are particularly noteworthy given the temporal and spatial contrast

168   between data sets (CALIOP = 2º latitude x 2º longitude bins from 2008 – 2017; zooplankton nets

169   at HOT and BATS from 1994 – 2005[21] and 1994 – 2017, respectively). Thus, correspondence

170   between Δbbp (which includes DVM animals, surface-resident organisms, and suspended

171   particles) and animal-specific ADCP[22] [Fig. 3b] and net measurements [Fig. 3c,d] gives

172   confidence to the DVM signal detected by CALIOP.

173

174   The biomass-normalized Δbbp property reflects the relative strength of the DVM signal, whereas

175   DVM biomass (DVM_{CALIOP}) is more quantitatively related to the simple difference, bbp^{night} -

176   bbp^{day}. We estimated DVM_{CALIOP} from this difference as:

$$DVM_{CALIOP} = a \, (bbp^{night} - c \, bbp^{day}), \quad\quad\quad\quad (3)$$

178   where a is an empirical conversion factor between backscattering (m^{-1}) and biomass ($g\ m^{-2}$)

179   determined from BATS and CALIOP data and c accounts for night-day bbp differences from

180   growth rate and day length dependent variations in the phytoplankton diel cycle [Methods].

181   Application of (3) to the CALIOP record yields a global distribution in DVM_{CALIOP} [Fig. 4a] that

182   differs markedly from Δbbp [Fig. 2]. In particular, DVM_{CALIOP} is generally low in the subtropical

183   gyres and high in the nutrient-enriched tropical regions. Thus, while the relative contribution of

184   DVM animals to nighttime plankton communities is higher in clearer waters [Fig. 2], total DVM

185   biomass is greater in more productive regions where food availability is enhanced [Fig. 4a].

186   Indeed, annual average DVM_{CALIOP} for our PSO regions is highly correlated with passive ocean

187   color based estimates of net primary production ($r^2 = 0.80$, $p = 0.002$) [Fig. 4b, Methods].

188   Results for the high-latitude northern and southern regions are also consistent with this finding

189   [Fig. 4b]. Importantly, an increase in phytoplankton production yields a less than proportional

190   increase in DVM_{CALIOP}, as might be expected for migrating animals that may be multiple trophic

191   levels removed from the phytoplankton. Consequently, the night-day difference in bbp caused

192   by the phytoplankton diel cycle [Fig. 1b] generally increases more rapidly than the DVM signal

193   as productivity increases, resulting in negative Δbbp values in productive tropical regions [Fig.

194   2].

195

196   Evidence of long-term changes in zooplankton populations, often linked to climate oscillations,

197   has emerged from field time-series studies[22-27]. At the HOT site, field-measured DVM

198   zooplankton biomass increased on average 12.4 mg m^{-2} y^{-1} (38% decade^{-1}) between 1994 and

199   2005 (p = 0.04)[21]. The DVM_{CALIOP} record indicates that this trend continued (p = 0.05) at a rate

200   of 23% decade^{-1} from 2008 to 2017 [Fig. 4c, red star]. At BATS, an overall increasing trend of

201   7.4 mg m^{-2} y^{-1} (54% decade^{-1}) was reported for field observations from 1994 to 2011 (p <

202   0.01)[22]. Expanding this data set to 2017 and re-evaluating, we find DVM biomass increased

203   63% decade^{-1} from 1994 to 2007 (p = 0.01) and then decreased 28% decade^{-1} from 2008 to 2017

204   (p = 0.04). For this latter period, DVM_{CALIOP} data similarly suggest a decreasing trend (9%

205   decade^{-1}; p > 0.1) for the 2º x 2º bin encompassing the BATS site [Fig. 4c, blue star]. The global

206   coverage provided by CALIOP now allows the evaluation of DVM biomass temporal trends to

207   be greatly expanded. For example, subdividing our eight PSO regions [Fig. 3a] into 6º x 6º bins

208   and evaluating only those bins that remain within their respective regional boundaries throughout

209   the year [Extended Data Fig. 2] reveals decadal trends in DVM_{CALIOP} with coherent geographical

210   patterns [Fig. 4c]. Specifically, a predominance of increasing DVM animal biomass is observed

211   in the NPSG, SPSG, SASG, and SISG, whereas decreasing DVM biomass is indicated across

212   much of the tropical regions and the NASG. Moreover, DVM_{CALIOP} is positively correlated with

213   changes in phytoplankton production for most bins, but in the two tropical Atlantic regions the

214   correlations are counterintuitively inverse [Fig. 4c].

215

216   The power of a satellite lidar in studying marine animals lies in its unparalleled annual coverage

217   of the global ocean. By contrast, it was necessary here to compile >30 years of ADCP

218   measurements to create a single field test data set and, even then, spatial and temporal coverage

219   is poor in many regions [Extended Data Fig. 4]. A challenge with satellite lidar data, however, is

220   that the measured night-day *bbp* differences are not solely due to DVM animals, so continued

221   work is needed to refine descriptions of the non-DVM contributors [Methods, Supplementary

222   Discussion]. Further field data analyses (*e.g.*, ADCP data, continuous plankton recorder survey

223   observations) and modeling[28] are also needed to fully understand the causative ecological

224   processes underlying the spatial and temporal DVM patterns observed from space, while an

225   advanced satellite lidar with ocean profiling capabilities[11] may contribute new insights on DVM

226   behaviors [Supplementary Discussion]. While there are clearly multiple new avenues to pursue

227   regarding the study DVM animals, results presented here provide a forward step in the global

228   exploration of this greatest animal migration on Earth.

229

230   1. Lampert, W. The adaptive significance of diel vertical migration of zooplankton. *Funct.*

231   *Ecol.* **3,** 21-27 (1989).

232

233   2. Hays, G. C. A review of the adaptive significance and ecosystem consequences of

234   zooplankton diel vertical migrations. *Hydrobiol*, **503,** 163-170 (2003).

235

236   3. Cuvier, G. Le règne animal distribué d'après son organisation pour à l'histoire naturelle des

237   animaux et d'introduction à l'anatomie compare. Deterville (1829).

238

239   4. Bianchi, D. & Mislan, K.A.S. Global patterns of diel vertical migration times and velocities

240   from acoustics data. *Limnol. Oceanogr*. **61,** 353-364 (2015).

241

242 5. Røstad, A., Kaartvedt, S. & Aksnes, D.L. Light comfort zones of mesopelagic acoustic

243   scattering layers in two contrasting optical environments. *Deep Sea Res. I* **113,** 1-6 (2016).

244

245 6. Steinberg, D.K., Goldthwait, S.A. & Hansell, D.A. Zooplankton vertical migration and the

246   active transport of dissolved organic and inorganic nitrogen in the Sargasso Sea. *Deep-Sea*

247   *Res. I* **49,** 1445–1461 (2002).

248

249 7. Bianchi, D., Stock, C., Galbraith, E.D. & Sarmiento, J.L. Diel vertical migration: Ecological

250   controls and impacts on the biological pump in a one-dimensional ocean model. *Global*

251   *Biogeochem. Cycl.* **27,** 478-491 (2013).

252

253 8. Steinberg, D.K. & Landry, M.R. Zooplankton and the ocean carbon cycle. *Ann. Rev. Mar.*

254   *Sci.* **9,** 413-444 (2017).

255

256 9. Churnside, J.H., Wilson, J.J. & Tatarskii, V.V. Lidar profiles of fish schools. *Appl. Opt.* **36,**

257   6011–6020 (1997).

258

259 10. Churnside, J.H. & Thorne, R.E. Comparison of airborne lidar measurements with 420 kHz

260   echo-sounder measurements of zooplankton. *Appl. Opt.* **44,** 5504–5511 (2005).

261

262 11. Hostetler, C.A., Behrenfeld, M.J., Hu, Y., Hair, J.W., Schulien, J.A. Spaceborne lidar in the

263   study of marine systems. *Ann. Rev. Mar. Sci.* **10,** 121–47 (2018).

264

11

265   12. Burt, W. J., & Tortell, P. D. Observations of zooplankton diel vertical migration from high-

266   resolution surface ocean optical measurements. *Geophys. Res. Lett*. **45,**

267   doi.org/10.1029/2018GL079992, (2018).

268

269   13. Briggs, N.T., Slade, W.H., Boss, E. & Perry, M.J. Method for estimating mean particle size

270   from high-frequency fluctuations in beam attenuation or scattering measurements. *Appl. Opt*.

271   **52,** 6710-6725 (2013).

272

273   14. Behrenfeld, M.J., *et al.* Space-based lidar measurements of global ocean carbon stocks.

274   *Geophys. Res. Lett.* **40,** 4355–4360 (2013).

275

276   15. Behrenfeld, M.J., *et al.* Annual boom-bust cycles of polar phytoplankton biomass revealed

277   by space-based lidar. *Nature Geosci.* **10,** 118–22 (2017).

278

279   16. Stramski, D., Shalapyonok, A., & Reynolds, R. A. Optical characterization of the oceanic

280   unicellular cyanobacterium *Synechococcus* grown under a day-night cycle in natural

281   irradiance. *J. Geophys. Res.-Ocean*. **100,** 13295–13307 (1995).

282

283   17. DuRand, M. D., Green, R. E., Sosik, H. M., & Olson, R. J. Diel variations in optical

284   properties of *Micromonas pusilla* (Prasinophyceae). *J. Phycol*. **38,** 1132–1142 (2002).

285

286   18. Dall'Olmo, G., *et al.* Inferring phytoplankton carbon and eco-physiological rates from diel

287   cycles of spectral particulate beam-attenuation coefficient. *Biogeosci.* **8,** 3423-3439 (2011).

288

289 19. Kheireddine, M. & Antoine, D. Diel variability of the beam attenuation and backscattering

290   coefficients in the northwestern Mediterranean Sea (BOUSSOLE site). *J. Geophys. Res.*

291   *Oceans*, **119,** 5465–5482 (2014).

292

293 20. Ohman, M.D., Frost, B.W. & Cohen, E.B. Reverse diel vertical migration: an escape from

294   invertebrate predators. *Science* **220,** 1404-1407 (1983).

295

296 21. Hannides, C.C.S, *et al*. Export stoichiometry and migrant-mediated flux of phosphorus in the

297   North Pacific Subtropical Gyre. *Deep-Sea Res. I.* **56,** 73-88 (2009).

298 22. Steinberg, D.K., Lomas, M.W. & Cope, J.S. Long-term increase in mesozooplankton

299   biomass in the Sargasso Sea: Linkage to climate and implications for food web dynamics and

300   biogeochemical cycling. *Global Biogeochem. Cycl*. **26,** GB1004,

301   doi:10.1029/2010GB004026 (2012).

302

303 23. Richardson, A. J. In hot water: Zooplankton and climate change. *ICES J. Mar. Sci.* **65,** 279–

304   295 (2008).

305

306 24. Beaugrand, G., Reid, P.C., Ibanez, F., Lindley, J.A. & Edwards, M. Reorganization of North

307   Atlantic marine copepod biodiversity and climate. *Science* **296,** 1692–1694 (2002).

308

309 25. Piontkovski, S.A. & Castellani, C. Long-term declining trend of zooplankton biomass in the

310   Tropical Atlantic. *Hydrobiol*. **632,** 365–370 (2009).

311

312 26. Peterson, W. T. & Schwing, F.B. A new climate regime in northeast Pacific ecosystems.

313   *Geophys. Res. Lett*. **30,** 1896, doi:10.1029/2003GL017528 (2003).

314

315 27. Chiba, S.,Tadokoro, K.,Sugisaki, H. & Saino, T. Effects of decadal climate change on

316   zooplankton over the last 50 years in the western subarctic North Pacific. *Glob. Change*

317   *Biol*. **12,** 907–920 (2006).

318

319 28. Archibald, K., Siegel, D. A., & Doney, S. C. Modeling the impact of zooplankton diel

320   vertical migration on the carbon export flux of the biological pump. Global Biogeochemical

321   Cycles **33,** 181– 199 doi: 10.1029/2018GB005983 (2019).

322

323 29. Behrenfeld, M.J., Boss, E., Siegel, D.A. & Shea, D.M. Carbon-based ocean productivity and

324   phytoplankton physiology from space. *Global Biogeochem. Cycles* **19,** GB1006,

325   doi:10.1029/2004GB002299 (2005).

326

327 30. Siegel, D.A., *et al*. Regional to global assessments of phytoplankton dynamics from the

328   SeaWiFS mission. *Rem. Sens. Env*. **135,** 77-91 (2013).

329

330 **Supplementary Information** is linked to the online version of the paper at

331 www.nature.com/nature.

332

339

340   **Author Contributions**: M.J.B. designed the study. M.J.B., P.G., A. DP, W.B, Y.H, and R.T.O.

341   processed data and analyzed results. M.J.B., P.G., A.DP, and R.T.O. prepared display items.

342   M.J.B. wrote the manuscript with contributions from all authors.

Figure Legends

344

345   **Figure 1. Marine animal and phytoplankton influences on day-to-night changes in**

346   **particulate backscattering coefficients (*bbp*) and the biomass-normalized difference ratio**

347   **(Δ*bbp*).** (a) Ship-based time-series of *bbp* showing nocturnal spikes associated with DVM

348   animals and the general lack of these spikes during the day[12] [Methods]. Black line = complete

349   *bbp* record. Purple line = de-spiked baseline *bbp* record. (b) Typical diel cycle in *bbp* due to

350   phytoplankton[19] [Methods]. Red dotted line = daily equator crossing times of CALIOP. (a – b)

351   Black and white bars on x-axis indicate night and day, respectively. (c) Biomass-normalized

352   difference ratios (Δ*bbp*) for ranges in DVM (x-axis) and phytoplankton (y-axis) contributions to

353   day-to-night *bbp* changes. For example, if the phytoplankton diel cycle corresponds (as in panel

354   b) to a 15% day-to-night decrease in *bbp* at the two CALIOP measurement times (horizontal

355   white dashed arrow) and this decrease is countered by a 5% increase in *bbp* from DVM animals

356   (vertical white dashed arrow), then Δ*bbp* will have a value of -10% (color inside labeled white

357   circle). Diagonal black lines correspond to the color bar range for the CALIOP observations

358   shown in figure 2. Note that values on the y-axis encompass the range of values expected in the

359   PSO [Supplementary Discussion, Extended Data Fig. 5].

360

361   **Figure 2. Global climatological signal of vertically migrating animals quantified as the**

362   **normalized difference ratio, Δ*bbp*.** Data are 2º latitude by 2º longitude bin averages for the

363   2008 to 2017 CALIOP record. Yellow/black line = contour of annual average sea surface

364   temperature of 15ºC, which effectively separates high-latitude seasonal seas from lower latitude

365   permanently stratified oceans.[29-30] Heavy black lines separate major regions of the PSO, where

366   the five subtropical gyres are defined by annual average surface chlorophyll concentrations of ≤

367   0.08 mg m^{-3}. Dark gray = excluded pixels where water column depth < 1000 m.

368

369   **Figure 3. Comparison of CALIOP normalized difference ratios (Δ*bbp*) and field-based**

370   **DVM measurements in the PSO.** (a) Color-coded regions of the PSO from figure 2. Yellow

371   stars = locations of the Hawaii Ocean Time-series (HOT) site and Bermuda Atlantic Time Series

372   (BATS) site. (b) CALIOP (Δ*bbp*) versus field ADCP (ΔB_{ADCP}) normalized difference ratios. Red

373   line = two-sided least squares linear regression fit to all 5° latitude x 5° longitude bins within our

374   eight PSO regions (slope = 0.42, F test p value = 0.001, n = 331 independent geographical bins)

375   [Supplementary Discussion]. Symbols = regional average values of Δ*bbp* and ΔB_{ADCP}, with

376   standard error bars shown for each region (n for each region = 19 for SISG, 18 for SASG, 115

377   for TP, 16 for NASG, 23 for NTA, 59 for NPSG, 22 for STA, 59 for SPSG, 302 for Other) .

378   Symbol colors identify region (labeled on right) and correspond to coloring in (a). For

379   completeness, the average value for all PSO bins outside our eight primary regions is indicated

380   by the white symbol. Numbers next to each symbol indicate the median number of days with

381   ADCP data within the 32 year field record for the bins within a given region. Dashed line is

382   two-sided least squares linear regression fit to regionally-averaged data for the n = six primary

383   regions where ΔB_{ADCP} is significantly greater than zero (slope = 0.64, r^2 = 0.55, p = 0.09). (c)

384   Average monthly field-measured (1994 – 2005)[21] migratory zooplankton biomass (g m^{-2} dry

385   weight) for the HOT site [Methods] (n = 112 net haul samples) and CALIOP-measured Δ*bbp*

386   (2008-2017) (n = 75 monthly retrievals) for a 2° latitude x 2° longitude bin centered on the HOT

387   site. Vertical lines indicate 1 standard deviation. Field and CALIOP data are offset on the x-axis

388   by 6 days to separate standard deviation lines. (d) Same as in (c) except for field (1994-2017) (n

389   = 285 net haul samples) and CALIOP (n = 87 monthly retrievals) data at the BATS site.

390

391   **Figure 4. CALIOP-based estimates of vertically migrating animal biomass (DVM_{CALIOP})**

392   **and temporal changes.** (a) Annual average DVM_{CALIOP} (g m^{-2} dry weight). Yellow-black and

393   heavy-black lines as in figure 2. (b) Relationship between annual average regional DVM_{CALIOP}

394   and mixed layer net primary production (NPP_{CbPM}, mg C m^{-3} d^{-1}) [Methods]. Solid line = two-

395   sided least squares linear regression fit (r^2 = 0.80, F test p value = 0.002, n = 9 geographic

396   regions) for the PSO regions, which are color-coded following figure 3a. Black symbols = high-

397   latitude North Pacific (NP), North Atlantic (NA), and Southern Ocean (SO) (see panel c). Error

398   bars = 1 standard deviation for annual values between 2008 and 2017 (n = 111 months per

399   geographic region). (c) Rate of change in DVM_{CALIOP} (% decade^{-1}) for 6° latitude x 6° longitude

400   bins for eight PSO regions and at the HOT and BATS sites (colored stars). Only bins that stay

401   within their respective regional boundaries throughout the year are shown [Extended Data Fig.

402   2]. Black dot in center of bin indicates trend is significant (two-sided least squares linear

403   regression, F test p value p < 0.05, n = 111 months per bin). Outlined bins exhibit a significant

404   (two-sided least squares linear regression,F test p value < 0.05, n = 111 months per bin)

405   relationship between DVM_{CALIOP} and NPP_{CbPM}, with black and green outlines indicating positive

406   and negative correlations, respectively.

407 **Methods**

408

409 **Field data in Figure 1:** Data shown in figure 1a provide five examples from the subarctic

410 Pacific where DVM animals significantly increased ship-measured *bbp* at night. Data are from

411 (12), which also provides full details on the study region, measurement system, data processing,

412 and uncertainty analyses. The phytoplankton diel cycle in *bbp* shown in figure 1b is from (19)

413 and is normalized to 1 at the nighttime minimum [Supplementary Discussion].

414

415 **CALIOP data:** CALIOP is the primary instrument on the Cloud-Aerosol Lidar and Infrared

416 Pathfinder Satellite Observation (CALIPSO) platform, which was launched in 2006 (31).

417 CALIOP measures the total time-dependent return of a pulsed laser output at 1064 nm and both

418 the co-polarized and cross-polarized return of a 532 nm laser output. The current study is based

419 on night and day differences in the cross-polarized return at 532 nm. *bbp* values (available at

420 http://www.science.oregonstate.edu/ocean.productivity/) were calculated from this signal

421 following (15), except that *bbp* at 532 nm was not converted to *bbp* at 440 nm as in the earlier

422 study. For (15), 30° off-nadir CALIOP tilting maneuvers were conducted every two weeks

423 between 2015 and 2016 to collect ocean measurements with minimal surface backscatter from a

424 wide range of ocean environments. Removing molecular backscatter from the CALIOP parallel

425 channel and combining with data from the cross-polarized channel, we then derived particulate

426 backscatter depolarization ratios and compared these data to collocated MODIS diffuse

427 attenuation (K_d) values. This analysis yielded a linear relationship between CALIOP

428 depolarization ratios and K_d that was then used in (15) to directly retrieve *bbp* values from

429 CALIOP without reliance on collocated MODIS observations. This same approach was used for

430   the current study. However, we also further evaluated the relationship between particulate

431   depolarization ratios and K_d at 532 nm using an extensive open ocean airborne lidar data set

432   compiled from the 2012 Azores campaign[14], the Ship-Aircraft Bio-Optical Research (SABOR)

433   campaign, and three campaigns of the North Atlantic Aerosol and Marine Ecosystem Study

434   (NAAMES)[32] (note, no airborne data were collected during the fourth NAAMES campaign due

435   to mechanical issues grounding the plane). This airborne-based analysis confirmed the earlier

436   CALIOP-MODIS finding of a linear relationship between depolarization ratios and K_d, with an

437   average depolarization:K_d of 1.76 m and standard deviation of 0.19 m. Finally, we calculated

438   *bbp* using a volume scattering function (VSF) at 180º following Lu et al.[33] that was developed

439   using measurements from collocated CALIPSO and MODIS 531 nm data. This VSF is

440   consistent with scattering properties for particles in the phytoplankton size domain and it was

441   applied to both day and night CALIOP data. Organisms larger than phytoplankton, such as

442   DVM animals, will have a VSF with a somewhat lower efficiency in the backward direction and

443   enhanced efficiency in the forward direction. This difference is one factor [see also

444   Supplementary Discussion] influencing the relationship between the CALIOP-retrieved DVM

445   backscatter signal and the biomass of these animals, but it is encompassed in the field-based

446   scaling factor between CALIOP bbp^{night} - bbp^{day} data and zooplankton dry weight (see below).

447

448   CALIOP merges low gain and high gain data onboard to reduce data downlink. The onboard

449   gain ratio calculations fail when there are not enough data for both the low and high gain

450   channels, which can happen for nighttime cross polarization measurements. At the beginning of

451   the CALIPSO mission, there was an error in the default values of the gain ratios when the

452   onboard calculation fails. This issue rendered the nighttime cross polarization measurements

453   unusable for ocean *bbp* retrievals until the error was corrected in late 2007, which is why the

454   current study on night-day differences in *bbp* was limited to the period of 2008 to 2017. In

455   addition, Advanced Microwave Scanning Radiometer (AMSR) data were used to flag and omit

456   CALIOP retrievals made at wind speeds $\geq$ 9 m s^{-1} to avoid bubble contamination of the *bbp*

457   values. At wind speeds < 9 m s^{-1}, we also applied a depolarization ratio threshold to remove

458   bubble-contaminated data based on statistical analysis from high wind conditions.

459

460   **Calculation of DVM_{CALIOP}:** The biomass of DVM animals (DVM_{CALIOP}) was estimated from

461   CALIOP-measured night-day differences in *bbp*, an estimate of the day-to-night change in *bbp*

462   due to the phytoplankton diel cycle alone [Fig. 1b], and a scaling factor between backscattering

463   and zooplankton dry weight.

464

465   The value of bbp^{night} can be expanded into backscatter by DVM animals (bbp^{DVM}) and

466   backscatter by phytoplankton and other non-migrating particles (bbp^{other}):

$$bbp^{night} = bbp^{DVM} + bbp^{other} . \qquad (4)$$

468   The value of bbp^{other} is equal to bbp^{day} corrected for the phytoplankton-based change (*c*) in *bbp*

469   from day to night. Rearranging (4) and solving for bbp^{DVM} yields:

$$bbp^{DVM} = bbp^{night} - c \, bbp^{day} . \qquad (5)$$

471   A variety of factors may influence the value of *c*, including the daily division rate of the

472   phytoplankton population, the degree to which this division is synchronized around the day-night

473   cycle, the composition of the phytoplankton community[34], and day length. Over much of the

474   PSO, phytoplankton populations are dominated by *Prochlorococcus*, *Synechococcus*, and

475   picoeukaryotics species, all of which generally synchronize cell division to the first half of the

21

476 night[35-39]. We therefore focused on describing c as a function of both division rate (μ; divisions

477 day^{-1}) and day length.

478

479 First, the dependence of c on μ was determined from the laboratory study of DuRand and

480 Olson[34] and is described by [Supplementary Discussion; Extended Data Fig. 5a]:

481 $$c_1 = 0.929 - 0.122 \; \mu \; , \tag{6}$$

482 where the term -0.122 has units of days division^{-1}. Equation 6 was applied to MODIS passive

483 ocean color based estimates of μ calculated for the 2008 to 2017 period (see below). Second, the

484 dependence of c on day length exists because a change in day length causes the two CALIOP

485 sampling points (determined by its fixed orbit) to line up differently with the phytoplankton diel

486 cycle. For the range of day lengths encountered across the PSO, this day length (dl) dependence

487 is described by [Supplementary Discussion; Extended Data Fig. 5b]:

488 $$c_2 = 0.986 + 0.0012 \; dl, \tag{7}$$

489 where dl (h) is known precisely for each CALIOP pixel based on date and latitude and the term

490 0.0012 has units of h^{-1}.

491

492 Monthly DVM zooplankton dry weight data are available at the BATS site over the 2008 to 2017

493 CALIOP era. Comparison of these field data to monthly bbp^{DVM} values calculated from

494 equations (5) through (7) for the 2° latitude by 2° longitude CALIOP bin centered on the BATS

495 site yields an average scaling factor between bbp^{DVM} and DVM biomass of 1596 g m^{-1}

496 [Supplementary Discussion]. Applying this conversion factor gives the following expression for

497 DVM_{CALIOP}:

498 $$DVM_{CALIOP} = 1596 \; (bbp^{night} - c_1 \; c_2 \; bbp^{day}). \tag{8}$$

499   In figures 3c and 3d, we compare HOT and BATS DVM zooplankton dry weight data to the

500   CALIOP-retrieved property, Δbbp, simply to maintain consistency with figure 3b

501   [Supplementary Discussion]. However and as stated in the main text, DVM biomass should be

502   quantitatively related to the simple difference, $bbp^{night} - bbp^{day}$. The reason the seasonal cycle in

503   Δbbp corresponds to that of DVM biomass at HOT and BATS is that bbp^{day} varies little over the

504   year at these two sites, making Δbbp highly correlated ($r^2 > 0.99$, $p < 0.001$) with the simple

505   difference, $bbp^{night} - bbp^{day}$.

506

507   **Field ADCP data:** Global ADCP data were obtained from the Joint Archive for Shipboard

508   ADCP (JASADCP, http://ilikai.soest.hawaii.edu/sadcp/). We selected acoustic backscatter data

509   for the upper 20 m of the ocean surface (equivalent to the sampling depth of CALIOP) from

510   ADCPs with frequencies of 150 or 300 kHz and excluded data from 38 and 75 kHz frequencies.

511   The 150 and 300 kHz frequencies better isolate scattering from the small (~0.5 – 5 mm) animals

512   that are most likely detected by CALIOP due to their much greater abundances. Backscatter

513   amplitude (E) measurements were converted into acoustic intensity (I_{dB}) following Gostiaux and

514   van Haren[40]:

$$I_{dB} = 10\log(10^{k_c E/10} - 10^{k_c\,E_{noise}/10}), \qquad\qquad (4)$$

516   where k_c is a scaling factor used to convert backscatter amplitude counts to decibels (dB), and

517   E_{noise} is the noise floor of the individual ADCP dataset. Values of k_c are frequency dependent

518   and were taken from Gostiaux and van Haren[40]. The noise floor was defined as the minimum

519    $k_c E$ for each individual data file. A total of 7,622 individual paired diel cycles were extracted

520   from the global database [Extended Data Fig. 4]. The geographic distribution of these diel cycle

521   data is largely biased to the regions surrounding the Hawaiian Islands, along the Tropical Ocean

522   Atmosphere (TAO/TRITON) mooring array in the equatorial Pacific, the Southern California

523   Bight, between Chile and Antarctica, and off the northeast United States seaboard [Extended

524   Data Fig. 4]. Detailed inspection of echograms computed from each individual data file revealed

525   occasional time synchronicity issues, with the apparent deep DVM occurring more than 2 hour

526   before or after local sunrise/sunset. To validate the time stamp of each data file, we compared

527   the timing of the mesopelagic (max depth of the data file to 150 m) DVM to the time of local

528   sunrise and sunset. Time synchronicity issues were detected in less than 10% of the data files.

529   The time stamp of these errant ADCP backscattering observations were corrected to synchronize

530   the deep DVM with sunrise/sunset prior to computing the day/night differences analyzed in the

531   manuscript.

532

533   **Field time-series zooplankton biomass data:** Monthly climatological migratory zooplankton

534   dry weight data shown in figure 3c for HOT were calculated from data in figure 1 of Hannides et

535   al[21]. Monthly climatological migratory zooplankton dry weight data shown in figure 3d for

536   BATS were calculated from 1994 to 2017 data provided by D.K.S. The 1994 to 2011 subset of

537   these data were published as figure 2c in Steinberg et al.[22].

538

539   **Global phytoplankton net primary production, biomass, and division rate data:**

540   Phytoplankton net primary production (*NPP*) values used for figure 4b,c, phytoplankton division

541   rates (μ) used for calculating c_1 in equation 6, and phytoplankton biomass (*C_{phyto}*) shown in

542   Extended Data Figure 6 are from the Carbon-based Production Model (*CbPM*)[41] using MODIS

543   passive ocean color data collected between 2008 and 2017 (data are available at

544   http://www.science.oregonstate.edu/ocean.productivity/).

545 **Author Information**: Reprints and permissions information is available at

546 www.nature.com/reprints. The authors declare no competing financial interests. Correspondence

547 and requests for materials should be addressed to MJB.

548

549 **Data Availability:** The CALIOP lidar and field ADCP datasets analyzed during the current

550 study are available at http://www.science.oregonstate.edu/ocean.productivity/ and from the Joint

551 Archive for Shipboard ADCP at http://ilikai.soest.hawaii.edu/sadcp/. Data presented in figures

552 3b-d and 4b and Extended Data figures 3, 6, 7, and 8 were provided as spate tabs in an excel file

553 as part of this manuscript submission.

554

555 31. Winker, D. M., *et al*. Overview of the CALIPSO Mission and CALIOP Data Processing

556   Algorithms. *J. Atmos. Ocean Tech.* **26,** 2310-2323 (2009).

557

558 32. Behrenfeld, M.J. *et al*. The North Atlantic Aerosol and Marine Ecosystem Study

559   (NAAMES): Science motive and mission overview. *Frontiers Mar. Sci.* **6,** 122. doi:

560   10.3389/fmars.2019.00122 (2019).

561

562 33. Lu, X., *et al.* Retrieval of ocean subsurface particulate backscattering coefficient from space-

563   borne CALIOP lidar measurements. *Opt. Express*, **24**, 29001-29008 (2016).

564

565 34. DuRand, M.D. & Olson, R.J. Diel patterns in optical properties of the chlorophyte

566   *Nannochloris* sp.: Relating individual-cell to bulk measurements. *Limnol. Oceanogr.*, **43,**

567   1107–1118 (1998).

568

569   35. Vaulot, D., Marie, D., Olson, R. J., & Chisholm, S.W. Growth of *Prochlorococcus*, a

570   photosynthetic prokaryote in the equatorial Pacific ocean. *Science* **268,** 1480–1482 (1995).

571

572   36. André J.M., Navarette, C., Blanchot, J., & Radenac, M.H. Picophytoplankton dynamics in

573   the equatorial Pacific: growth and grazing rates from cytometric counts. *J. Geophys. Res*.

574   **104,** 3369–80 (1999).

575

576   37. Vaulot, D. & Marie, D. Diel variability of photosynthetic picoplankton in the equatorial

577   Pacific. *J. Geophys. Res. - Ocean* **104,** 3297-3310 (1999).

578

579   38. Binder, B.J. & DuRand, M.D. Diel cycles in surface waters of the equatorial Pacific. *Deep-*

580   *Sea Res. II* **49,** 2601–2617 (2002).

581

582   39. Jacquet, S., Prieur, L., Avois-Jacquet, C., Lennon, J. F., & Vaulot, D. Short-timescale

583   variability of picophytoplankton abundance and cellular parameters in surface waters of the

584   Alboran Sea (western Mediterranean). *J. Plankt. Res.* **24,** 635–651 (2002).

585

586   40. Gostiaux, L. & Van Haren, H. Extracting meaningful information from uncalibrated

587   backscattered echo intensity data. *J. Atmo. Ocean. Techn.* **27.5,** 943-949 (2010).

588

589   41. Westberry, T.K., Behrenfeld, M.J., Siegel, D.A., & Boss, E. Carbon-based primary

590   productivity modeling with vertically resolved photoacclimation. *Global Biogeochem. Cycles*

591   **22,** GB2024, doi:10.1029/2007GB003078 (2008).

26

592 **Extended Data Figure Legends**

593 **Extended Data Figure 1: Global CALIOP observational coverage**. (a-e) CALIOP ground

594 tracks for (a) one, (b) two, (c) four, (d) eight, and (e) sixteen days. (f) Number of months for each

595 2° latitude x 2° longitude bin with day and night retrievals of *bbp* for the 2008 and 2017 study

596 period. Total number of months possible is 115. The north-south strip of low retrieval success

597 in the middle of the Pacific is caused by a gap in ancillary AMSER surface wind data, which is

598 used for flagging data with potential bubble contamination [Methods].

599

600 **Extended Data Figure 2: Global distributions of monthly climatological average values of**

601 **Δ*bbp*.** Thin black line = contour of monthly average sea surface temperature of $15^{\circ}C$. Heavy

602 black lines = Monthly extent of the five subtropical gyres where annual average surface

603 chlorophyll concentrations are ≤ 0.08 mg m^{-3}.

604

605 **Extended Data Figure 3: Time series of Δ*bbp* for the PSO.** (a-h) 2008 to 2017 monthly

606 values of Δ*bbp* (%) for the eight PSO regions (labeled at top of each panel) identified in figure 3a

607 of the main manuscript.

608

609 **Extended Data Figure 4: Global coverage of field ADCP data.** Number of days within each

610 5° latitude by 5° longitude bin that paired day-night ADCP data are available from the 1985 to

611 2017 JASADCP-based field archive (http://ilikai.soest.hawaii.edu/sadcp/). Total number of days

612 possible is 11,680. White bins = no data. Yellow/black line = contour of annual average sea

613 surface temperature of $15^{\circ}C$. Heavy white lines = boundaries of the eight PSO regions identified

614 in figure 3a of the main manuscript.

615

Extended Data Figure 5: Influence of phytoplankton division rate and of day length on calculated DVM backscatter for the PSO. (a) Values for c_1 (see equation 6 in Methods of main manuscript) over the range of phytoplankton division rates (μ) in the PSO (n = 999 monthly μ values for all PSO regions). Solid circle = mean value of μ and c_1 for the PSO. Box = ±1 standard deviation from the mean value of μ. (b) Values for c_2 (see equation 7 in Methods of main manuscript) over the range of day lengths in the PSO (n = 999 monthly day length values for all PSO regions). Solid circle = mean day length and c_2 value for the PSO. Box = ±1 standard deviation from the mean day length.

624

Extended Data Figure 6: Seasonal cycles in monthly mean regionally-integrated values of DVM_{CALIOP} (g m^{-2}) and phytoplankton biomass (C_{phyto}; mg C m^{-3}) for high-latitude regions. (a) North Pacific. (b) North Atlantic. (c) Southern Ocean. These three regions are identified in figure 4c of the main manuscript. Vertical lines = ±1 standard deviation (n = 111 monthly DVM_{CALIOP} and C_{phyto} values for each region). C_{phyto} data are from the Carbon-based Production Model (*CbPM*) and MODIS passive ocean color data [Methods].

631

Extended Data Figure 7: Comparison of CALIOP night-day *bbp* differences and field ADCP night-day differences in acoustic backscatter. Dashed line = two-sided least squares linear regression fit to data for the SPSG, NPSG, TP, STA, NASG, and NTA (n = 6). For completeness, the average value for PSO bins outside our eight primary regions is indicated by the white symbol. Symbols = regional average values with standard error bars (n for each region = 19 for SISG, 18 for SASG, 115 for TP, 16 for NASG, 23 for NTA, 59 for NPSG, 22 for STA,

638   59 for SPSG, 302 for Other). Symbol colors identify region (labeled on right) and correspond to

639   coloring in figure 3a of the main manuscript. Numbers next to each symbol indicate the median

640   number of days with ADCP data within the 32-year field record for the 5° latitude x 5° longitude

641   bins.

642

643   **Extended Data Figure 8: Bin-to-bin comparison of CALIOP Δ*bbp* and field-based DVM**

644   **measurements in the PSO.** (a) CALIOP normalized difference ratios (Δ*bbp*) versus field

645   ADCP (ΔB_{ADCP}) normalized difference ratios for 5° latitude x 5° longitude bins within the PSO.

646   Black line = two-sided least squares linear regression fit. Black line = two-sided linear least

647   squares regression relationship (F test p value for slope < 0.001, n = 331 independent

648   geographical bins) for all data from our eight primary PSO regions (colored symbols, labeled on

649   right). White symbols = PSO values for 5° x 5° bins outside of the eight primary regions.

650   Inclusion of these data in the linear regression analysis increases to the F test p-value to 0.005 (n

651   = 633 independent geographical bins). (b) Relationship between field DVM biomass at the HOT

652   site measured for a given calendar month and year (x-axis) versus DVM biomass measured

653   during all other years for the same calendar month (y-axis).

654

655   **Extended Data Figure 9: Field-based diel cycles in *bbp*.** Average diel cycles in *bbp* from

656   Kheireddine and Antoine[19] for (blue line) mixing (n = 69 days of measurements), (green line)

657   oligotrophy (n = 322 days of measurements), and (red line) declining (n = 32 days of

658   measurements) conditions and (black line) the average of these three cycles, which corresponds

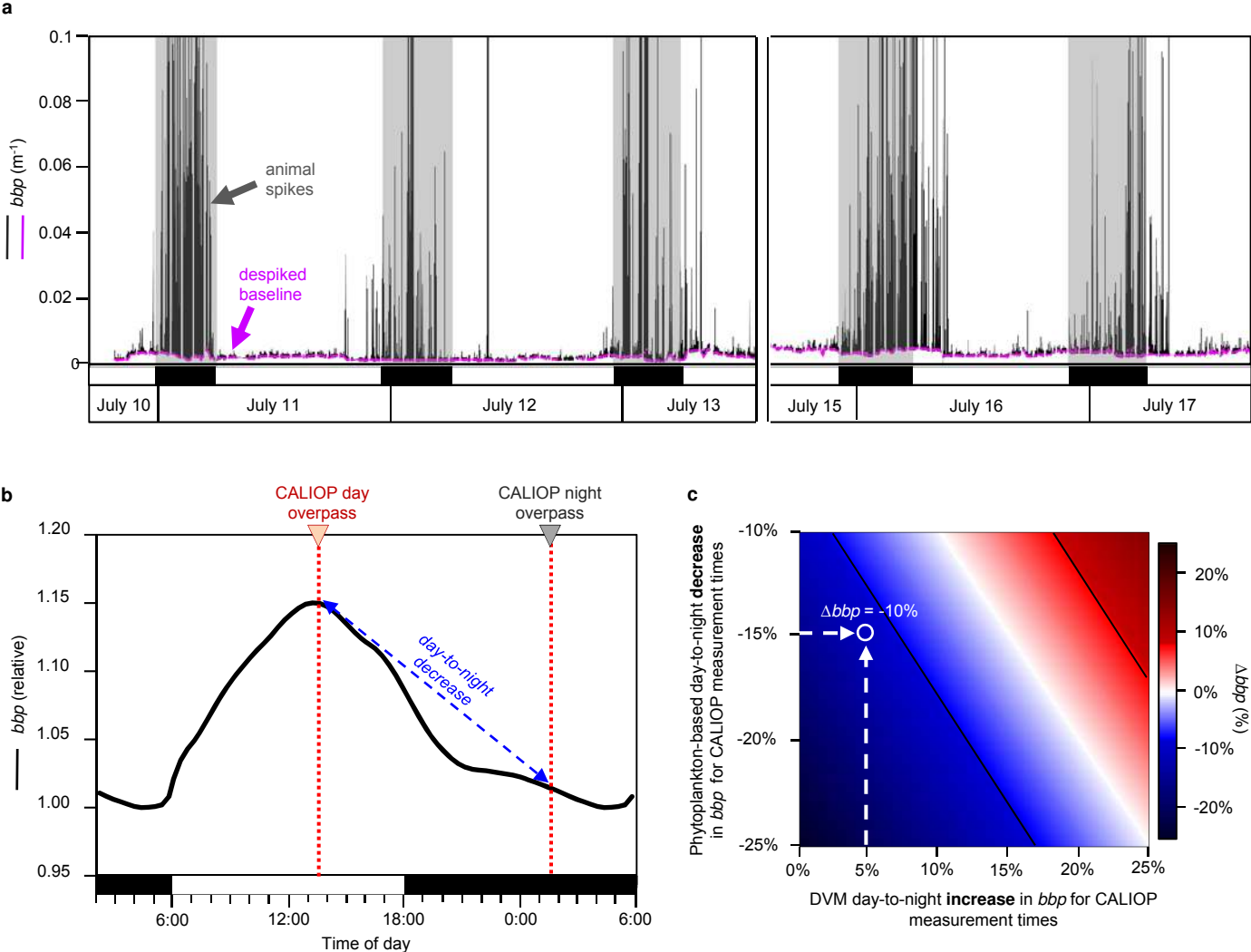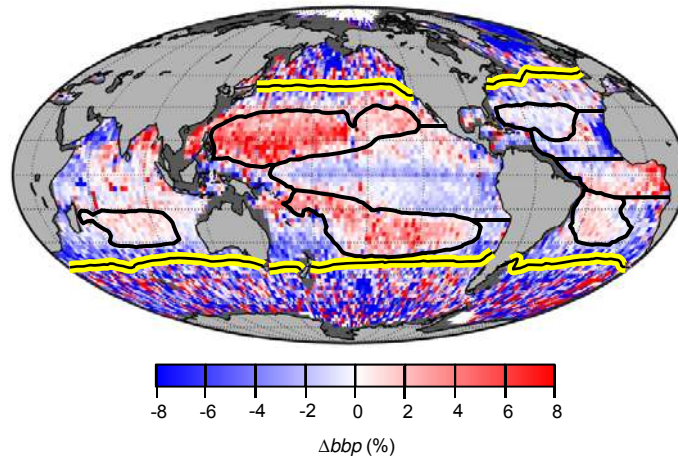659   to the diel cycle in Fig. 1b of the main manuscript.

Figure 1

a

b
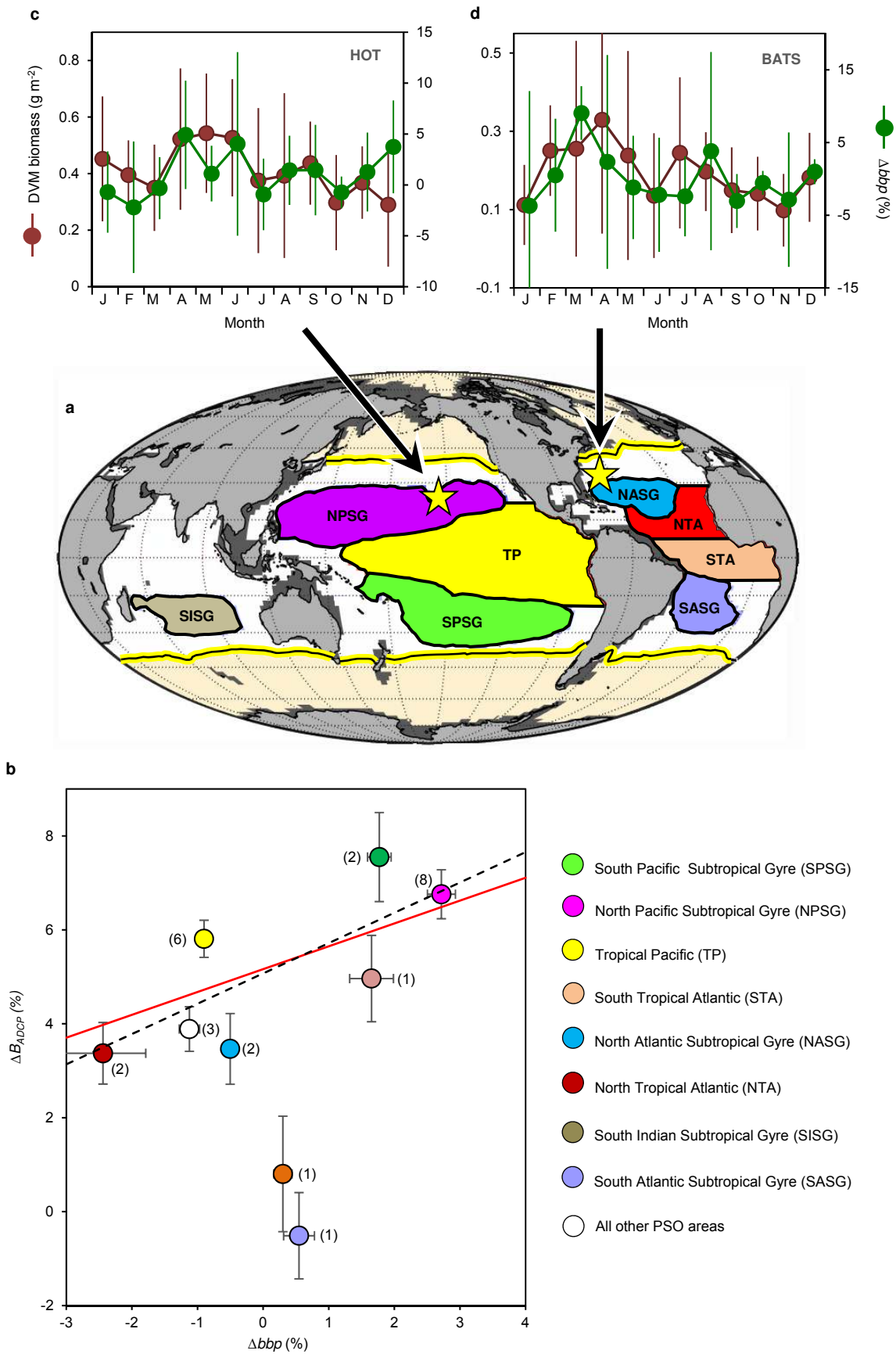

c

Figure 2

Δbbp (%)

Figure 3

Figure 4

a

b

c

= DVM_{CALIOP} significantly (p < 0.05) and positively correlated with NPP_{CbPM}

= DVM_{CALIOP} significantly (p < 0.05) and negatively correlated with NPP_{CbPM}

no outline = DVM_{CALIOP} and NPP_{CbPM} not significantly (p > 0.05) correlated
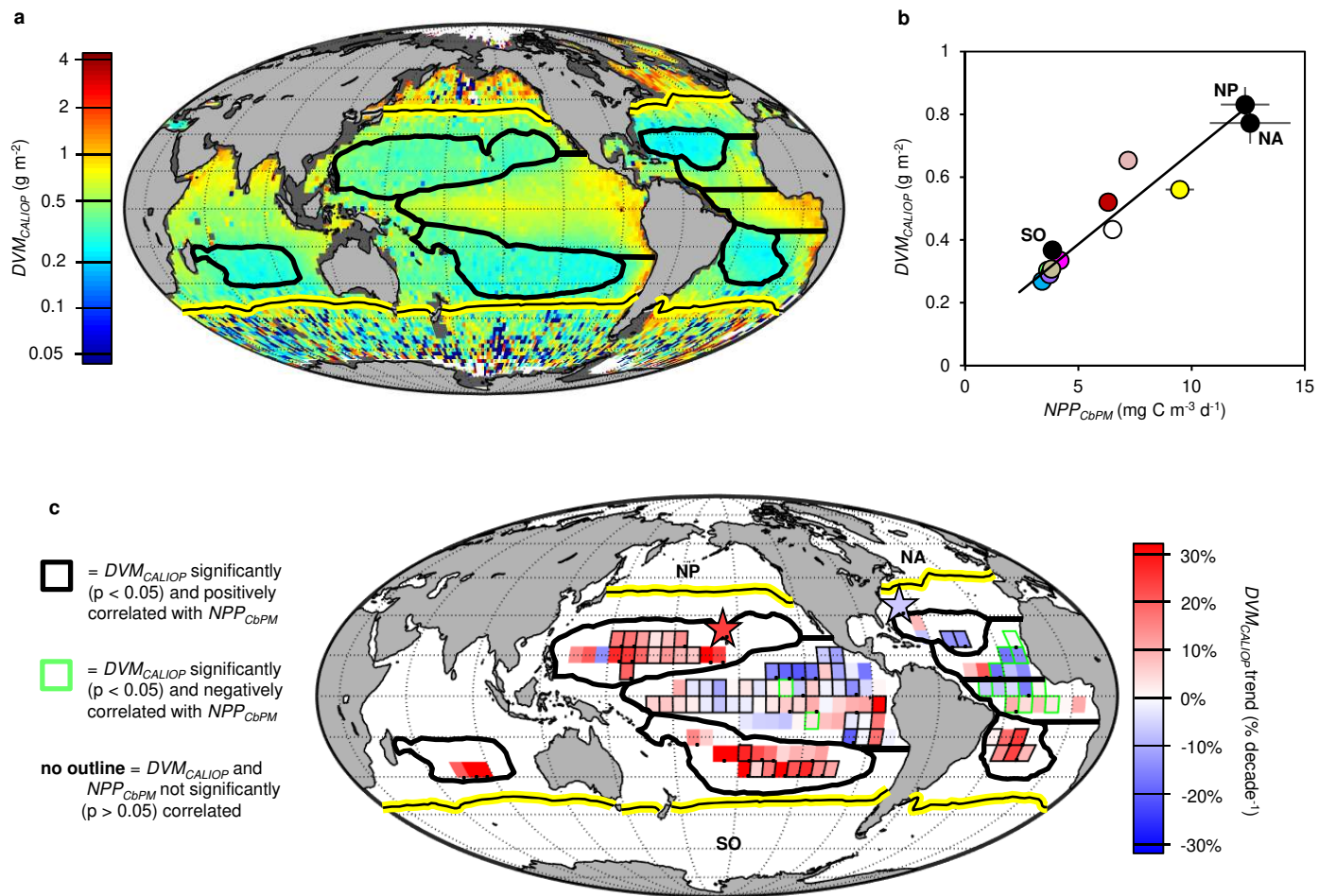
Supplementary Discussion

This file includes supplemental text for the manuscript, "Satellite-observed daily vertical migrations of global ocean animals", by Behrenfeld *et al*. regarding (1) CALIOP orbits and data binning, (2) high-latitude spatial variability in CALIOP retrievals, (3) normalized difference ratio data and results in figure 3 of the main manuscript, (4) calculation of the phytoplankton diel *bbp* cycle, (5) additional details on calculations of DVM biomass, and (6) directions for future research.

1) CALIOP orbits and data binning: While satellite lidar measurements have become a common tool for atmospheric research, they are relatively new for studying ocean ecosystems[11,14,15]. Unlike familiar passive ocean color instruments that use a rotating telescope or 'push-broom' approach to achieve broad-swath measurements, the CALIOP instrument conducts its measurements at a near-nadir angle and only along its orbit tracks, which are oriented along the ground in opposite directions on the daylight and dark sides of the Earth. Extended Data Figure 1a shows day and night orbits for a single 24 hour period, illustrating how rare orbit cross-over points are for collecting spatially coincident data within a single day (and ocean retrievals for many of these will be prevented by clouds). Furthermore, even when ocean retrievals are successful at both times for a given cross-over point, the water sampled during the day will be different than that measured 12 hours later at night because surface waters are continuously moved by ocean currents. Because of these considerations, we used binned CALIOP data to evaluate global patterns in DVM animals rather than focusing only on spatially coincident data. Binning was also necessary for comparing CALIOP results to field data (which are also spatially and temporally sparse).

While not providing broad swaths of data like an ocean color sensor, advantages of CALIOP are that it provides measurements during the day and night and its rapid laser pulse rate enables measurements every 330 m along the ground. In addition, its precessing orbit allows for fully-global sampling over its 16-day repeat cycle. Extended Data Figures 1a-e illustrate how this global coverage builds-up over 1, 2, 4, 8, and 16 days. Thus, for a given spatial binning resolution, the CALIOP approach can provide a dense within-bin 'sampling' over the course of a month. Averaging these repeated measurements within a monthly bin reduces noise in the retrieved ocean property and allows the signal of interest to be isolated. As discussed in **Section 2** below, the number of successful day and night retrievals within a bin depends on atmospheric conditions (cloud cover, aerosol thickness), which vary strongly with latitude.

In our first publication using CALIOP data[14], we validated satellite-retrieved *bbp* values using coincident ship-based and airborne-based field measurements. We then binned global CALIOP data into 2° latitude $\times$ 2° longitude bins to evaluated global patterns in phytoplankton biomass and total particulate carbon concentration. The same $2^o \times 2^o$ binning was used in the current manuscript for figure 2. In our second CALIOP publication[15], we demonstrated an excellent agreement between CALIOP and ocean color based seasonal cycles in *bbp* and then used $1^o \times 1^o$ binned data to evaluate phytoplankton bloom dynamics. This slightly higher spatial resolution was used because the study was geographically restricted to the north and south polar regions, whereas $2^o \times 2^o$ binning is appropriate for the global scope of the current study. For figure 3b of the current manuscript, a coarser resolution of $5^o \times 5^o$ was used because of the very sparce coverage of ADCP data. Finally, $6^o \times 6^o$ binning was used for figure 4c because (1) smaller bins

make it difficult to distinguish the outlines and dots used for each bin that indicate statistical significance and (2) the enhanced signal-to-noise of the larger bins improves detection of temporal trends (i.e., de-seasoned anomalies) in DVM_{CALIOP}.

2) High-latitude zones: At latitudes poleward of the PSO, CALIOP retrievals of the DVM signal remain noisy between the spatial bins used for our analysis. In contrast, these retrievals exhibit significantly better spatial coherence within the PSO. Consequently, we have largely restricted our more detailed analyses of the CALIOP record to these lower-latitude PSO regions. A number of factors contribute to the noisy spatial maps of the DVM signal at high latitudes. First and foremost of these factors is the combined impact of spatial and temporal variability in plankton ecosystems, persistent cloudiness, and the sampling coverage of CALIOP. Extended Data Figure 1f shows the total number of months within the 2008 – 2017 period (115 total possible) for each 2° latitude x 2° longitude bin with at least one day and one night retrieval of *bbp*. This latter figure clearly shows the much poorer coverage at high latitudes, but even this stark difference between high latitudes and the PSO over-represents high-latitude coverage. CALIOP's small single-shot footprint (100 m at the ocean surface) allows successful retrievals between even small gaps in cloud cover. Thus, even if a given bin is largely overcast for an entire month (as is often the case at higher latitudes), a single day and night retrieval through gaps in the clouds would yield a day-night pair for that month and add to the total number of measurement pairs for that bin in Extended Data Figure 1f. These two points could come from different locations anywhere within the 2° x 2° bin and may be separated in time by nearly a month. In such a case, spatial and temporal variations in the plankton community can be a large contributor to the calculated night-day difference. As cloudiness decreases from this extreme

example, many more CALIOP retrievals can be averaged together within a given 2º x 2º bin, thereby dampening the influence of plankton community spatial and temporal variations and better isolating the DVM signal (as discussed above). In the PSO, clear sky scenes are far more common than at higher latitudes. With a 100 m single-pulse footprint and a 330 m ground distance separation between pulses, >600 measurements can be collected within a given 2º x 2º bin on a single day or night overpass under clear skies. With clear sky conditions for even two overpasses per month, this means that >1200 daytime measurements and >1200 nighttime measurements spanning the breadth of the bin may be available to calculate a single monthly average night-day difference. In addition, temporal variability in plankton stocks within the 2º x 2º bins of the PSO tend to be smaller than most high-latitude bins. Thus within the PSO, effective retrieval of the DVM signal at 2º × 2º binning resolution is far more likely than at higher latitudes. One solution to the 'spatial speckling' problem at high latitudes is to average data over a much larger area. When we do this, we find that regionally-integrated annual average DVM_{CALIOP} for the three high-latitude regions shows a relationship with annual average mixed layer net primary production that is highly consistent with that found for the PSO regions [Fig. 4b]. Furthermore, regionally-integrated monthly DVM_{CALIOP} data for the three high-latitude regions exhibit strong annual cycles consistent with both the magnitude and seasonality of phytoplankton biomass in these regions [Extended Data Fig. 6].

In addition to the above considerations regarding high latitude retrievals, phytoplankton community composition in these regions tends to be more diverse than in the PSO, division rates vary strongly with season and are poorly constrained by satellite productivity algorithms, and it is highly likely that cell division cycles are often not synchronized to the daily light-dark cycle.

The impact of these ecological considerations on the phytoplankton night-day difference is currently unresolved (see **Section 6** below).

3) Normalized difference ratios: In figure 2 of the main manuscript, we compare CALIOP retrievals of Δbbp with normalized difference ratios calculated from field ADCP measurements. We used normalized difference ratios (equations 1 and 2 in the main manuscript) for this comparison for two primary reasons. First, division of night-day differences by daytime values makes the retrieved property biomass-specific, allowing an evaluation of the relative contribution of DVM animals. Second, normalization to daytime values, at least in part, helps reduce the influence of instrument-dependent variations in the field measurements. Specifically, the ADCP acoustic backscatter record used in the current study was compiled from more than 30 research vessels and 2,000 field surveys. Differences between the instruments used, how they are mounted, and how they are calibrated can generate instrument-dependent differences in the resultant backscattering data that are not linked to real differences in *in situ* particle backscattering. By calculating the normalized difference ratio, the influence of this instrument-dependent contribution is reduced. To illustrate the significance of this normalization, the ADCP-CALIOP comparison presented in figure 3b of the main manuscript was revised by substituting the normalized difference ratios with simple differences (i.e., y-axis = $I_{dB}^{night} - I_{dB}^{day}$; x-axis = $bbp^{night} - bbp^{day}$) for each data set [Extended Data Fig. 7]. The outcome of this analysis is similar to the result presented in figure 3b of the main manuscript. Specifically, (1) the relative location of each regional average value is the same between graphs and (2) results for the SISG and SASG regions deviate from the other regions in the same manner in both graphs.   The primary difference (as expected from the above discussion) is that the linear regression on the

regional ADCP and CALIOP values shown in figure 3b gives an $r^2 = 0.55$ and $p = 0.09$, whereas the same comparison for data in Extended Data Fig. 7 gives an $r^2 = 0.39$ and $p > 0.10$.

In figures 3c and 3d, we also compare Δbbp to DVM biomass measured at the HOT and BATS sites. The expectation is that, across the PSO, DVM biomass will be more quantitatively related to the simple difference, $bbp^{DVM} = bbp^{night} - c\ bbp^{day}$, than the normalized difference ratio. Since bbp^{DVM} and Δbbp have nearly the exact same seasonal cycle at HOT and BATS ($r^2 = 0.99$, $p < 0.001$), we chose to show the CALIOP normalized difference ratio data in figures 3c and 3d simply to be consistent with figure 3b. However, as described in the main manuscript, the actual calculation of DVM biomass is based on the simple difference, bbp^{DVM}.

As discussed in the main text and in the Methods section, creating an adequate field data set (with respect to PSO coverage) for comparison with CALIOP data required aggregating historical ADCP data from over 30 years (1985 to 2017). Even over this long period, most of our 5° x 5° bins have only one to a few days of data, and many of these observation pre-date CALIOP. Due to this paucity of data and their temporal mismatches with CALIOP, figure 3b in the main manuscript focuses on the correspondence between regional values of ΔB_{ADCP} and Δbbp. However, we also report that linear regression analysis of ΔB_{ADCP} and Δbbp data for all 5° x 5° bins within the eight primary PSO regions yielded a highly significant slope similar to the relationship calculated from the regionally binned data. Extended Data Fig. 8a shows this relationship, where data are color-coded following the regional coloring scheme shown in figure 3a of the main manuscript. As expected, the relationship for all individual data exhibits significant scatter around the least squares linear regression line ($r^2 = 0.04$). We can use the

HOT time series field measurement of DVM biomass to put this result in context. Specifically, we can ask how much predictive skill does knowledge of DVM biomass during a given month of a given year provide in estimating DVM biomass for the same month but other years in the HOT record. This result is shown in Extended Data Fig. 8b. The implication here is that there is a large amount of year-to-year variability in monthly DVM biomass within field records and thus considerable scatter is expected between CALIOP and field ADCP data when compared at the level of individual measurements [Extended Data Fig. 8a], particularly when the two data sets are collected during different years. However, when data are averaged over time and space, clear regional differences emerge in DVM strength and these patterns are consistent between the ADCP and CALIOP records for all PSO regions except the SASG and SISG [Fig. 3b] (see **Section 6** below). A corollary to this result is found in the published studies of Hannides et al.[21] and Steinberg et al.[22], where an annual cycle in DVM biomass becomes clear by calculating monthly average values for field records extending a decade or more. Because of the large variability between years in the monthly data [e.g., Extended Data Fig. 8b], these cycles are difficult to decipher in the full time-series records.

4) Phytoplankton diel *bbp* cycle: Historical studies on diel cycles in ocean inherent optical properties have largely focused on the particulate beam attenuation coefficient[42-44]. To our knowledge, the only published account of diel cycles in *bbp* are from Kheireddine and Antoine[19]. In their study, five years of *bbp* data were evaluated from the long-term, deep-water (2440 m) BOUSSOLE buoy site in the Mediterranean Sea. Over this period, 1322 total days of data were collected, from which the authors selected 737 days of highest data quality. These data were then separated into mixing, declining, oligotrophic, and bloom-climax phases with respect to

phytoplankton biomass. A vast majority of the data were from the three former phases, which are most representative of the PSO. The average diel cycle in *bbp* for each of these phases is reproduced as the blue, red, and green lines, respectively, in Extended Data Fig. 9. The average of these three diel cycles is shown as the black line in Extended Data Fig. 9 and this averaged cycle corresponds to the diel cycle shown in figure 1b of our main manuscript. The bloom-climax data in (19) exhibits a similar diel cycle as during the other seasons but with a daytime peak ~2 hour later in the afternoon.

5) DVM biomass calculations: The biomass of DVM animals (DVM_{CALIOP}) was calculated from CALIOP-measured night (bbp^{night}) and day (bbp^{day}) differences in *bbp* following [Eq. 3 of main manuscript]:

$$DVM_{CALIOP} = a\ (bbp^{night} - c_1\ c_2\ bbp^{day}),$$

where c_1 accounts for growth rate (μ; divisions day^{-1}) dependent night-day differences in *bbp* due to the phytoplankton diel cycle [Fig. 1b], c_2 accounts changes in night-day *bbp* differences caused by variations in day length, and *a* is an empirical conversion factor between the backscatter signal of DVM animals (bbp^{DVM}) and zooplankton biomass. In the following three subsections, we provide details on the derivation of c_1, c_2, and *a*.

For the current study, we did not attempt to introduce an additional correction factor to account for community composition effects on the phytoplankton diel *bbp* cycle because (1) community composition is relatively conserved in the open ocean regions of the PSO (at least compared to higher latitude and coastal regions), (2) very little is known from targeted field or laboratory studies about taxonomic influences on the diel *bbp* cycle, and (3) satellite-based global

determinations of phytoplankton community composition are still relatively immature and would likely add more errors than improvements in our estimates of DVM_{CALIOP}. Beyond taxonomic considerations, we also evaluate whether regional time series in bbp^{night} - bbp^{day} covaried with other globally-retrieved ocean properties (surface chlorophyll a concentration, euphotic zone depth, median mixed layer light level, surface PAR, mixed layer depth, sea surface temperature), but found no unique relationships consistent across regions that could not be attributed to corollary relationships between these other ocean properties and variations in phytoplankton growth rates.

Dependence on division rate: Very few controlled studies have been conducted that enable a quantitative assessment of growth rate dependent variability in the phytoplankton diel bbp cycle. One notable exception is the study of DuRand and Olson[34]. In that study, diel cycles in scattering cross section were reported for cultures of *Nannochloris* (chosen as representative of the small phytoplankton found in oligotrophic waters) grown under daily light-dark irradiance cycles of intensity ranging from 60 to 1500 µmole photons m^{-2} s^{-1}. Cell division cycles in all cultures were tightly phased with the light:dark cycle, with division occurring in the dark (as is the case in the PSO). The relationship between growth irradiance and μ (divisions day^{-1}) was extracted from figure 3 of DuRand and Olson[34]. Daytime maxima and nighttime minima in scattering cross section were extracted for each growth condition from figure 6 of DuRand and Olson[34]. The relationship between these minimum and maximum values and values that would be observed during the CALIOP measurement times was calculated using the field-based diel cycle in figure 1b of the current manuscript (see **Section 4** above). A two-sided least squares linear regression analysis was then conducted on the relationship between the night-day

difference in these scattering values and μ ($r^2 = 0.40$, $p = 0.12$, $n = 6$). However, this relationship does not provide a description of c_1 because it is based on a pure phytoplankton culture, whereas *bbp* data from CALIOP includes additional 'background' scattering from other non-phytoplankton components. This issue was addressed by considering the results presented in figure 1b where the field-measured diel cycle in *bbp* gives a day-to-night decrease in *bbp* of ~15%. These field data were collected in the Mediterranean Sea where the dominant prokaryotic and picoeukaryotic phytoplankton divide at a rate slightly less than 1 division day^{-1}. Thus, assuming a bulk phytoplankton division rate of ~0.8 division day^{-1}, a 'background' *bbp* signal was added to our DuRand and Olson[34] based two-sided linear regression result until a value for c_1 of 0.85 was achieved for $\mu = 0.8$ division day^{-1}. This resultant description for c_1 is:

$$c_1 = 0.929 - 0.122\,\mu.$$

The mean, standard deviation, and range for c_1 values in the PSO are shown in Extended Data Fig. 5a.

Dependence on day length: The dependence of c on day length exists because a change in day length causes the two CALIOP sampling points (determined by its fixed orbit) to line up differently with the phytoplankton diel cycle. To account for this effect, the field-based diel cycle in *bbp* shown in figure 1b was split into its daytime and nighttime components. The duration of these day and night components was then expanded and contracted to create diel cycles for day lengths ranging from 4 to 20 hours (i.e., outside this range both CALIOP measurement times either occur in the day or the night). The night-day difference in *bbp* was then calculated for the two CALIOP measurement times for each day length. For the highly constrained range in day length across the PSO (10 – 14 h), the relationship between these night-

day difference values and day length is linear ($r^2 = 1.0$, $p < 0.001$). This relationship was then

adjusted to give a value of 1 for a 12:12 day:night cycle (i.e., the day length corresponding to the

data in figure 1b). The resultant relationship is:

$$c_2 = 0.986 + 0.0012 \; dl,$$

where dl = day length (h). The mean, standard deviation, and range for c_2 values in the PSO are

shown in Extended Data Fig. 5b, with the full range being highly constrained to $c_2 = 0.998$ to

1.002. Thus, inclusion of c_2 in our calculation of DVM biomass is more for completeness than

as an important correction in the calculation of DVM_{CALIOP}.

Over a broader range of day lengths, the relationship between night-day difference values and

day length becomes nonlinear and, when normalized to 1 for a 12:12 day:night cycle is described

by ($r^2 = 1.0$, $p < 0.001$):

$$c_2 = -7\text{E-}06 \; dl^4 + 0.0004 \; dl^3 - 0.0069 \; dl^2 + 0.06 \; dl + 0.8013,$$

which for a day length range of 4 to 20 hours gives a slightly larger range of values for c_2 of

0.952 to 1.006.

Scaling bbp^{DVM} to DVM_{CALIOP}: Our primary motivation for scaling bbp^{DVM} to DVM_{CALIOP} was to

convert the former property with units of m^{-1} into a more ecologically-understandable property

with units of g m^{-2} dry weight. For this conversion, we use a constant scaling factor, meaning

that the results shown in figure 4 of the main manuscript can be interchanged between the

directly-measured CALIOP property, bbp^{DVM}, and the scaled biomass property, DVM_{CALIOP}. Our

approach for quantifying the scaling factor between bbp^{DVM} to DVM_{CALIOP} was similar to that

used for more standard satellite ocean color products, such as surface chlorophyll concentration.

Specifically, we used field data collected coincidently (in this case at the monthly time scale) with CALIOP. For the current study, this means that we limited our analysis to BATS field data collected between 2008 and 2017, which yielded a conversion factor of 1596 g dry weight m^{-1}. If we had instead combined these BATS data with monthly average DVM biomass data from HOT (1994 to 2005) adjusted for the apparent 23% increase since the end of the field record (see main manuscript), then the resultant conversion factor would have been 1402 g dry weight m^{-1}.

6) **Future directions:** The current manuscript describes the first attempt to connect a satellite-retrieved property (*bbp*) to animal biomass and distributions in the global ocean. As is standard practice in satellite oceanography, we have used the best available *in situ* observations (ADCP and zooplankton biomass time-series data) to validate the CALIOP retrievals before attempting an interpretation of their ecological meaning. As should be expected with any such new satellite product, additional future studies and new technologies are needed to both evaluate and constrain uncertainties in our analysis and to expand upon the capabilities of CALIOP for studying global ocean DVM animals. The following list provides some examples.

    i.   *Phytoplankton diel bbp cycle*: CALIOP retrieved Δ*bbp* span from negative to positive values because nighttime increases in *bbp* from DVM animals are countered by a background phytoplankton diel cycle that decreases *bbp* from day to night. We have used data from the only published study that has quantified the phytoplankton diel *bbp* cycle in the field[19]. These data were collected at a single location in the Mediterranean Sea and, while a range of phytoplankton populations were encountered during that study, similar analyses are needed in other ocean regions with different phytoplankton

populations to evaluate the robustness of our description of phytoplankton diel *bbp*

changes. These analyses should include populations where cell division of the dominant

species are synchronized over the diel cycle and also populations where cell division is

not synchronized, as the latter case is likely common at higher latitudes.

It is important to recognize that the assessment of phytoplankton diel *bbp* cycles in the

field is not as straightforward as it might initially appear. The problem is that the cycle of

interest is the biomass-normalized cycle, so an appropriate (preferably independent)

assessment of biomass is needed, particularly when measurements are conducted on a

moving ship. One potential approach is to divide *bbp* by coincident measurements of

chlorophyll concentration, but this approach will typically fail because cellular

chlorophyll concentrations also have a diel cycle of their own that will result in an

incorrect cycle for biomass-normalized *bbp*. In the study of Kheireddine and Antoine[19],

measurements were conducted from a fixed location (rather than a moving ship) and *bbp*

values measured over each diel cycle were normalized to the value measured at dawn.

However, even for this study, physical advection of the surface layer ensures that

different populations were sampled over each diel cycle, which may largely be the reason

that this earlier study typically found that *bbp* values at the end of a given diel cycle were

not the same as at the beginning[19]. A great advantage of the Kheireddine and Antoine[19]

study was that investigators had a large number of daily cycles in *bbp* to work with and

thus, through averaging, they arrived at consistent cycles under various growth conditions

(see **Section 4** above).

An alternative approach for addressing uncertainties in the phytoplankton diel *bbp* cycle would be to conduct a series of laboratory experiments (much like that of DuRand and Olson[34]) where different phytoplankton species are synchronized to light-dark cycles of various durations and changes in *bbp* are continually monitored over the diel cycle. Such experiments should also encompass a range in growth rates for each species to enable development of predictive relationships.

ii. *DVM biomass*: In the current study, we convert CALIOP retrievals of bbp^{DVM} into an estimate of DVM animal biomass using data from a single field time-series data set (i.e., BATS). This conversion was largely conducted to put CALIOP results in more intuitive ecological units (see **Section 5** above), but there is significant uncertainty in this single conversion factor. Specifically, the backscattering efficiency of DVM animals depends on animal size, shape, composition, and other factors and the CALIOP-coincident BATS time-series data do not encompass every type of DVM animal found in the global oceans. Achieving more accurate estimates of DVM_{CALIOP} from bbp^{DVM} will require a broader diversity of field samples, an increase in the number of time-resolved DVM animal properties characterized, and a detailed optical model linking these properties to backscattering.

iii. *Spatial sampling*: As discussed in detail above, spatial binning is required to achieve low-noise day-night match-up data with CALIOP. These binned data must then be validated with field observations that are typically collected at much smaller scales (e.g., the size of the opening of a zooplankton net or the footprint of a ship ADCP). A future

study is needed to assess uncertainties in this spatial disconnect by providing a direct

measurements that span the sampling scales of field zooplankton and CALIOP data. One

potential approach here would be to couple ship-based DVM animal and backscattering

measurements with airborne lidar measurements. In this scenerio, the airborne

measurements could be conducted along a flight pattern that encompasses the retrieval

scale of a satellite lidar, and might even be coordinated with simultaneous CALIOP

overpasses (as in Behrenfeld et al.[14]), assuming CALIOP is still operational.

iv. *South Indian and South Atlantic Subtropical Gyres*: When regionally-averaged field

ADCP and CALIOP data are compared [Fig. 3B, Extended Data Fig. 7], results for the

SISG and SASG deviate from the other PSO regions. Potential reasons for this

discrepancy are discussed in the main manuscript. Of particular concern is the low

number of ADCP data available for these two regions in the historical record and their

temporal disconnect with the CALIOP record. However, it is noteworthy that the

individual bin data for the SISG and SASG actually span a considerable fraction of the

range of variability in Δbbp and ΔB_{ADCP} found for the other PSO regions [Extended Data

Fig. 8a]. Clearly, additional field sampling campaigns are needed in the SISG and SASG

to investigate the underlying basis of the apparent discrepancy in regionally-averaged

Δbbp and ΔB_{ADCP} values.

v. *New technology*: CALIOP was designed for atmospheric science, not ocean applications.

It provides information on ocean *bbp* for only a single 22 m depth bin immediately below

the ocean's surface. High Spectral Resolution Lidar (HSRL) instruments have been

developed since the launch of CALIOP and extensively field demonstrated from aircraft over a diversity of ocean regimes. These instruments can retrieve *bbp* values deep within the sunlit surface layer of the ocean with meter-scale vertical resolution. If this technology is transferred to a satellite instrument, the HSRL approach could yield both improved accuracy in *bbp* retrievals and an assessment of DVM animal nighttime vertical distributions. It is conceivable that vertically resolved DVM retrievals could provide information on feeding behavior linked to phytoplankton production layers and more accurate assessments of DVM biomass, as only those DVM animals that reach the upper 22 m of the surface are currently detected by CALIOP.

References

42. Siegel, D.A., Dickey, T.D., Washburn, L., Hamilton, M.K., & Mitchell, B.G. Optical determination of particulate abundance and production variations in the oligotrophic ocean, *Deep Sea Res. Part A* **36,** 211–222, doi:10.1016/0198-0149(89)90134-9 (1989).

43. Stramski, D., Shalapyonok, A., & Reynolds, R. A. Optical characterization of the oceanic unicellular cyanobacterium *Synechococcus* grown under a day-night cycle in natural irradiance. *J. Geophys. Res.-Ocean.* **100,** 13295–13307 (1995).

44. Dall'Olmo, G., *et al.* Inferring phytoplankton carbon and eco-physiological rates from diel cycles of spectral particulate beam-attenuation coefficient. *Biogeosci.* **8,** 3423-3439 (2011).

Extended Data

This file includes all Extended Data for the manuscript, "Global satellite observations of vertically migrating animals in the ocean's surface layer", by Behrenfeld *et al*. This file includes the following materials:

1) **Extended Data Figure 1:** Global CALIOP ground tracks for (a) one, (b) two, (c) four, (d) eight, and (e) sixteen days. (f) Number of months for each 2º latitude x 2º longitude bin with day and night retrievals of *bbp* for the 2008 and 2017 study period. Total number of months possible is 115. The north-south strip of low retrieval success in the middle of the Pacific is caused by a gap in ancillary AMSER surface wind data, which is used for flagging data with potential bubble contamination [Methods].

2) **Extended Data Figure 2:** Global distributions of monthly climatological average values of Δ*bbp*. Thin black line = contour of monthly average sea surface temperature of 15ºC. Heavy black lines = Monthly extent of the five subtropical gyres where annual average surface chlorophyll concentrations are ≤ 0.08 mg m^{-3}.

3) **Extended Data Figure 3:** 2008 to 2017 monthly values of Δ*bbp* (%) for the eight PSO regions (labeled at top of each panel) identified in figure 3a of the main manuscript.

4) **Extended Data Figure 4:** Number of days within each 5º latitude by 5º longitude bin that paired day-night ADCP data are available from the 1985 to 2017 JASADCP-based field archive (http://ilikai.soest.hawaii.edu/sadcp/). Total number of days possible is 11,680. White bins = no data. Yellow/black line = contour of annual average sea surface temperature

of 15°C. Heavy white lines = boundaries of the eight PSO regions identified in figure 3a of the main manuscript.

5) **Extended Data Figure 5:** (a) Values for c_1 (see equation 6 in Methods of main manuscript) over the range of phytoplankton division rates (μ) in the PSO. Solid circle = mean value of μ and c_1 for the PSO. Box = ±1 standard deviation from the mean value of μ. (b) Values for c_2 (see equation 7 in Methods of main manuscript) over the range of day lengths in the PSO. Solid circle = mean day length and c_2 value for the PSO. Box = ±1 standard deviation from the mean day length.

6) **Extended Data Figure 6:** Monthly mean regionally-integrated values of DVM_{CALIOP} (g m^{-2}) and phytoplankton biomass (C_{phyto}; mg C m^{-3}) for the high-latitude (a) North Pacific, (b) North Atlantic, and (c) Southern Ocean regions identified in figure 4c of the main manuscript. Vertical lines = ±1 standard deviation. C_{phyto} data are from the Carbon-based Production Model ($CbPM$) and MODIS passive ocean color data [Methods].

7) **Extended Data Figure 7:** Comparison of CALIOP night-day bbp differences and field ADCP night-day differences in acoustic backscatter. Dashed line = two-sided least squares linear regression fit to data for the SPSG, NPSG, TP, STA, NASG, and NTA. For completeness, the average value for PSO bins outside our eight primary regions is indicated by the white symbol. Symbols = regional average values with standard error bars. Symbol colors identify region (labeled on right) and correspond to coloring in figure 3a of the main manuscript. Numbers next to each symbol indicate the median number of days with ADCP data within the 32-year field record for the 5° latitude x 5° longitude bins.
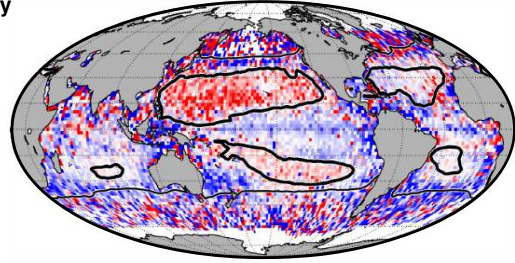
8) **Extended Data Figure 8:** (a) CALIOP normalized difference ratios (Δbbp) versus field

ADCP (ΔB_{ADCP}) normalized difference ratios for 5º latitude x 5º longitude bins within the

PSO. Black line = two-sided least squares linear regression fit. Black line = linear least

squares regression relationship (p-value for slope < 0.001, n = 331) for all data from our

eight primary PSO regions (colored symbols, labeled on right). White symbols = PSO values

for 5º x 5º bins outside of the eight primary regions. Inclusion of these data in the linear

regression analysis increases to the p-value to 0.005 (n = 633). (b) Relationship between

field DVM biomass at the HOT site measured for a given calendar month and year (x-axis)

versus DVM biomass measured during all other years for the same calendar month (y-axis).

9) **Extended Data Figure 9:** Average diel cycles in *bbp* from Kheireddine and Antoine[19] for

(blue line) mixing, (green line) oligotrophy, and (red line) declining conditions and (black

line) the average of these three cycles, which corresponds to the diel cycle in Fig. 1b of the

main manuscript.

one day

a
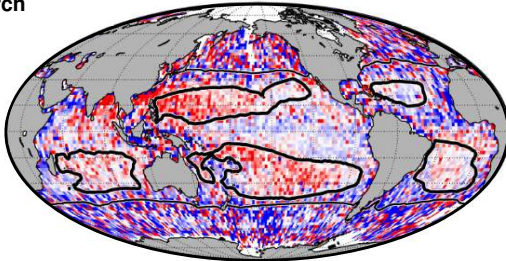
two day

b

four day

c

eight day

d

sixteen day

e

f

Number of months with paired
day and night retrievals

0   20   40   60   80   100
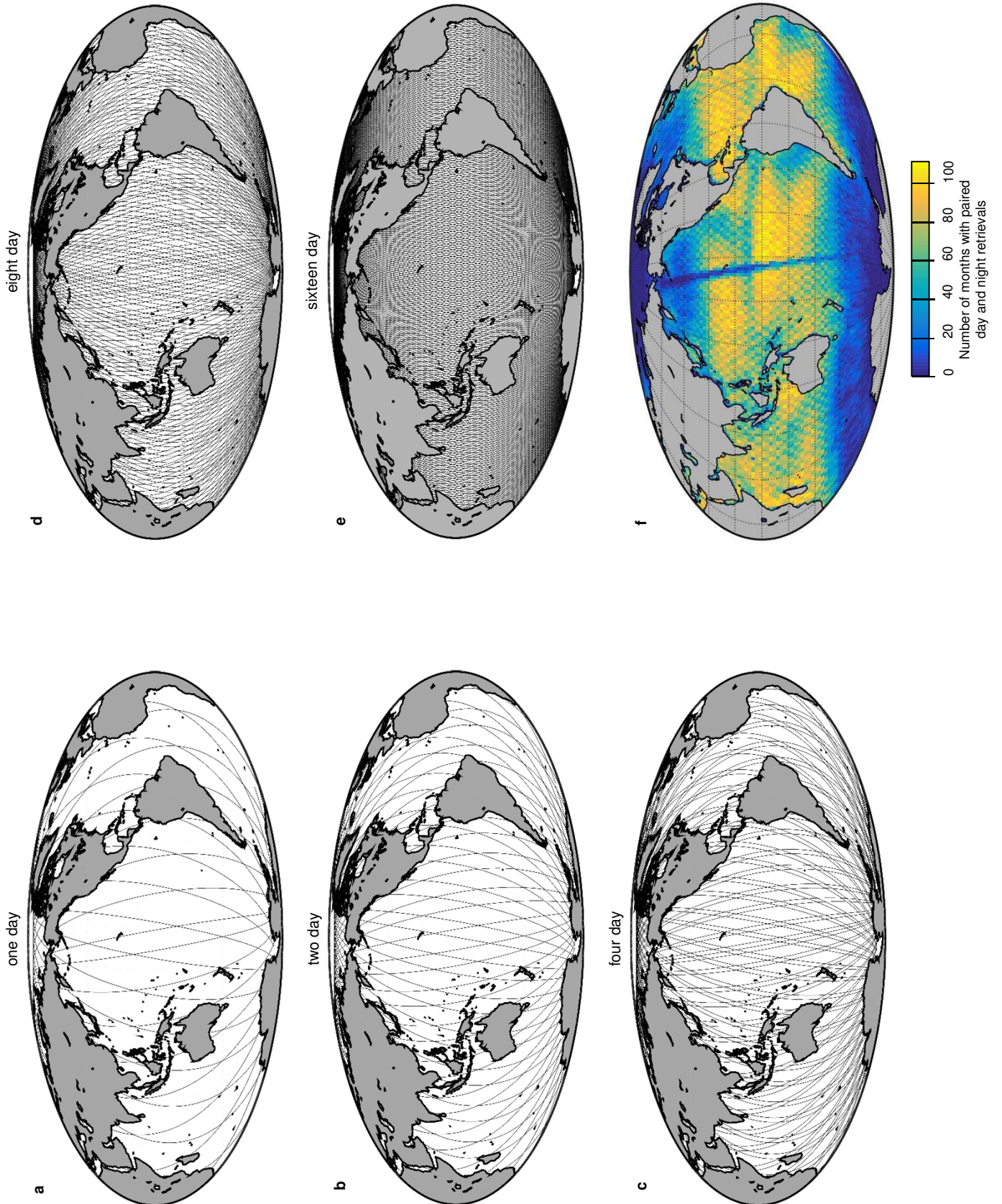
January
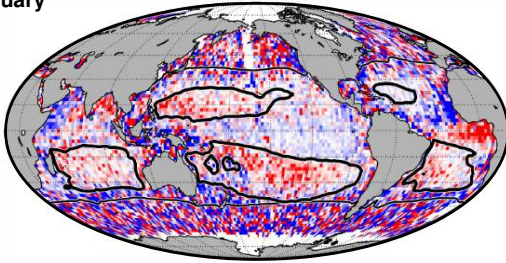
July

February
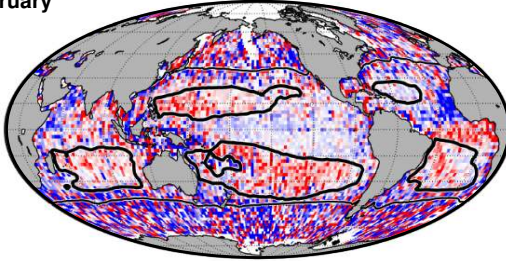
August
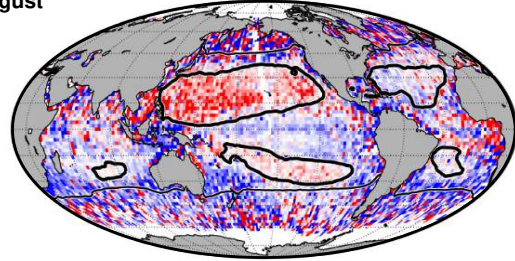
March

September
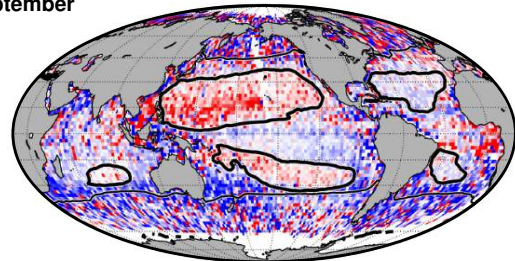
April
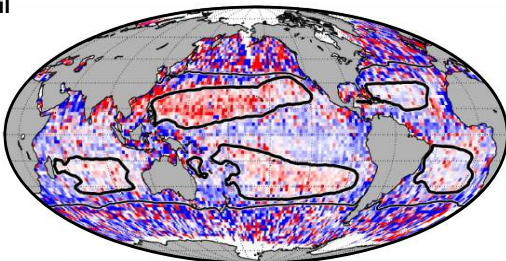
October
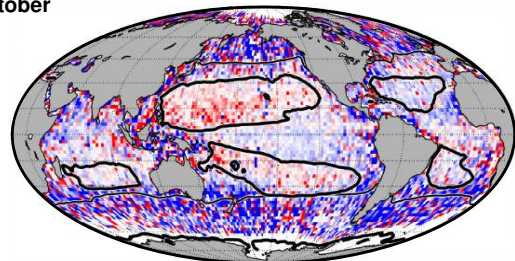
May

November

June

December

-10 -8 -6 -4 -2 0 2 4 6 8 10

Δ*bbp* (%)